

Weighing the Neutrinos with the Galaxy Shape-Shape Correlations

Jounghun Lee^{1,*} and Suho Ryu^{1,†}

¹*Department of Physics and Astronomy, Seoul National University, Seoul 08826, Republic of Korea*

The galaxies form and evolve in the early epochs through the anisotropic merging process along the primary narrow filaments, in the direction of which their shapes become elongated and intrinsically aligned. The non-linear evolution of the cosmic web broadens the primary filaments, by entangling them with multiple secondary filaments, which has an effect of reducing the anisotropy of the merging process and in consequence weakens the galaxy shape-shape correlations in the later epochs. Assuming that the degree of the nonlinearity and complexity of the cosmic web depends on the nature of dark matter, we propose a hypothesis that the galaxy shape-shape correlation function, $\eta(r)$, may be a powerful complimentary probe of the total neutrino mass, M_ν . Testing this hypothesis against a high resolution N-body simulation, we show that the M_ν -dependence of $\eta(r)$ at $z = 0$ is sensitive enough to distinguish between $M_\nu = 0.0$ eV and $M_\nu = 0.1$ eV. We also show that the differences in $\eta(r)$ at $r \leq 5 h^{-1}$ Mpc between the models with massless and massive neutrinos cannot be explained by their differences in the small-scale density powers, σ_8 , which implies that the galaxy shape-shape correlation function has a potential to break the notorious cosmic degeneracy between M_ν and σ_8 .

Introduction. The shapes of the Milky way-sized galaxies in the universe are observed to be mutually and intrinsically cross-correlated [1]. The recent numerical studies based on high-resolution cosmological simulations have suggested that the galaxy shape-shape correlations should be closely linked with the anisotropic merging process in the filamentary cosmic web, through which the galactic halos form and evolve [2]. In the early epochs, the galactic halos become elongated in the directions of the primary narrow filaments along which the merging events most frequently occur, and in consequence their shapes become mutually correlated over the scales comparable to the spatial extents of the primary filaments [2, 3].

In the later epochs, however, the cosmic web develops a more complex structure where the primary filaments entangled with multiple secondary filaments become broader than the sizes of the galactic halos [2]. In this nonlinearly evolved cosmic web, the merging process would occur more or less isotropically [4], which has an effect of diminishing the strength of the halo shape-shape correlations. Given that the presence of the cosmic web is caused by the large-scale coherence of the tidal shear fields [5], whose nonlinear evolution can be retarded by the free streaming of hot dark matter particles like massive neutrinos [6, 7], the degree of the nonlinearity and complexity of the cosmic web is expected depend on the nature of dark matter.

We claim here that the halo shape-shape correlations can be a new complementary probe of the relic neutrinos, which must possess non-zero mass according to the results of the solar neutrino oscillation experiments [see 8, for a review]. Our goal here is to numerically prove this claim by utilizing the data from recently available high-resolution N-body simulations performed for the $\nu\Lambda$ CDM cosmologies (the cosmological constant Λ + cold dark matter CDM + three species of neutrinos ν with the total mass, $M_\nu \geq 0.0$ eV).

Numerical Analysis and Results. The halo shape-shape cor-

relation function, $\eta(r)$, is defined as [9]

$$\eta(r) \equiv \langle |\hat{\mathbf{e}}(\mathbf{x}) \cdot \hat{\mathbf{e}}(\mathbf{x} + \mathbf{r})|^2 \rangle - \frac{1}{3}, \quad (1)$$

where $\hat{\mathbf{e}}(\mathbf{x})$ and $\hat{\mathbf{e}}(\mathbf{x} + \mathbf{r})$ denote the unit vectors in the major principal directions of the inertia momentum tensors of the DM halos located at the positions of \mathbf{x} and $\mathbf{x} + \mathbf{r}$, respectively. From here on, we call, $\hat{\mathbf{e}}$, a *shape vector of a DM halo*. The first term in the right-hand side of Equation (1) represents the ensemble average of the squares of the inner products between $\hat{\mathbf{e}}(\mathbf{x})$ and $\hat{\mathbf{e}}(\mathbf{x} + \mathbf{r})$, which is $1/3$ if there is no correlation.

To investigate the M_ν -dependence of $\eta(r)$, we utilize the publicly available data from the Cosmological Massive Neutrino Simulations (MassiveNuS) conducted by [10] for a number of $\nu\Lambda$ CDM models with diverse initial conditions. Performed in a periodic box of a side length $512 h^{-1}$ Mpc, the MassiveNuS has mass and particle resolutions as high as $10^{10} h^{-1} M_\odot$ and 1024^3 , respectively. In the MassiveNuS, the analytic linear response approximation was adopted to track down the positions and velocities of the relic neutrinos, while the Rockstar algorithm [11] was applied to the phase space distributions of the DM particles to find the distinct halos and their subhalos as well. The Rockstar catalog from the MassiveNuS provides information on various properties of each object including $\hat{\mathbf{e}}$, its position $\mathbf{x} = (x_i)$, minor-to-major axial ratio S , virial mass M_h and radius r_h , and scale radius r_s .

For the current scrutiny on the M_ν -dependence of $\eta(r)$, we consider only three $\nu\Lambda$ CDM models with massless, light and heavy neutrinos (corresponding to $M_\nu = 0.0, 0.1$ and 0.6 eV, respectively). For the three models, the key cosmological parameters, other than M_ν , such as the matter density parameter, baryon density parameter, amplitude of the primordial power spectrum, spectral index and dimensionless Hubble parameter are identically set at $\Omega_m = 0.3$, $\Omega_b = 0.047$, $A_s = 10^{-9}$, $n_s = 0.97$ and $h = 0.7$, respectively. Given these initial conditions, the values of the rms fluctuations of the linear density contrasts within a spherical radius $8 h^{-1}$ Mpc were evaluated to be 0.85, 0.83 and 0.74 for the $\nu\Lambda$ CDM models with massless, light and heavy neutrinos, respectively.

*Electronic address: jounghun@astro.snu.ac.kr

†Electronic address: ryu@snu.ac.kr

For each model, we make a sample of the well resolved distinct halos by eliminating the subhalos from the catalog of the Rockstar objects at $z = 0$ and selecting only those halos with $M_h \geq 10^{12} h^{-1} M_\odot$ containing 100 or more DM particles. For each pair of the distinct halos in the sample, we measure their separation distance r , and compute the square of the inner product between their shape vectors. Subtracting $1/3$ from its spatial average taken over those pairs of the distinct halos with r in the differential bin $[r, r + dr]$, we numerically determine $\eta(r)$. The ensemble average over the realizations in Equation (1) is replaced by the spatial average over \mathbf{x} , which can be justified by the ergodic theorem. To estimate the errors in the determination of $\eta(r)$ at a given r -bin to which n_{pair} pairs of the distinct halos belong, we generate n_{pair} sets of 10^6 random unit vectors and determine the one standard deviation scatter, σ_η , among the sets, as done in [12]. Finally, the errors in $\eta(r)$ at each r -bin is estimated to be $\sigma_\eta / \sqrt{n_{\text{pair}}}$.

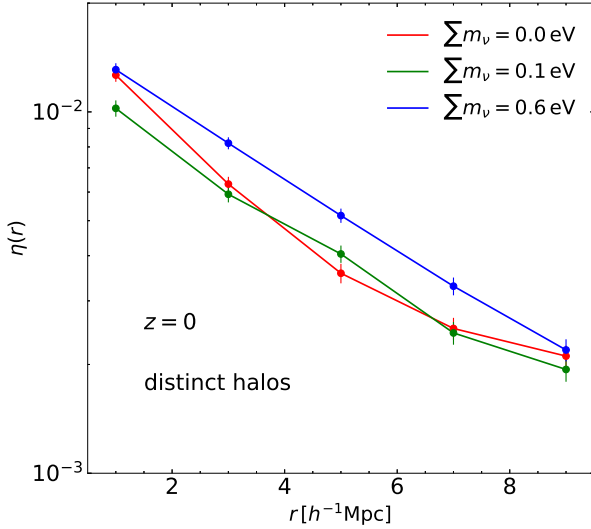


FIG. 1: Intrinsic shape-shape correlation function of the distinct DM halos from the MassiveNuS at $z = 0$ for three different $\nu\Lambda\text{CDM}$ models.

Figure 1 plots the numerically obtained $\eta(r)$ in the distance range of $r < 10 h^{-1}\text{Mpc}$ from the samples of the distinct halos at $z = 0$ for the three $\nu\Lambda\text{CDM}$ models. The results at longer distances $r \geq 10 h^{-1}\text{Mpc}$ are found to carry large uncertainties and thus left out. From here on, we let $\eta_{0.0}(r)$, $\eta_{0.1}(r)$ and $\eta_{0.6}(r)$ denote the halo shape-shape correlation functions from the models with massless, light and heavy neutrinos, respectively.

As can be seen, $\eta_{0.0}(r)$ shows a distinctly different behavior compared with $\eta_{0.1}(r)$ and $\eta_{0.6}(r)$. For the latter two functions, their M_ν -dependence shows a simple pattern, $\eta_{0.1}(r) > \eta_{0.6}(r)$ in the whole range of r , which is consistent with our expectation based on the following logic. In the model with heavy neutrinos that has a lower value of σ_8 than the model with light neutrinos, the shape-shape correlations of the galactic halos retain better the initial strengths that they acquired in

the early epochs through the preferential merger events along the narrow primary filaments.

Meanwhile, the difference between $\eta_{0.0}(r)$ and the other two functions shows a more complicated pattern. At $3 \leq r/[h^{-1}\text{Mpc}] < 8$, we find $\eta_{0.0}(r) \sim \eta_{0.1}(r) < \eta_{0.6}(r)$, which can be ascribed to the differences in σ_8 among the three models. However, at $r < 3 h^{-1}\text{Mpc}$, we witness a much more rapid increase of $\eta_{0.0}(r)$ with the decrement of r than $\eta_{0.1}(r)$ and $\eta_{0.6}(r)$, which leads $\eta_{0.1}(r) < \eta_{0.0}(r) \sim \eta_{0.6}(r)$ at $r \sim 1 h^{-1}\text{Mpc}$. This behavior cannot be explained by the aforementioned simple logic, since the two models with massless and heavy neutrinos have widely different values of σ_8 . Some other mechanism like the gravitational halo-halo interactions must counteract the effect of the high value of σ_8 to enhance $\eta_{0.0}(r)$ at $r \leq 2 h^{-1}\text{Mpc}$ only for the case of massless neutrinos.

In practice, what is more readily observable is not the correlations between the shapes of the distinct halos but the correlations between the projected shapes of the galaxies. We make a sample of the galactic halos in the mass range, $10^{12} \leq M/[h^{-1}M_\odot] < 10^{13}$, from the MassiveNuS Rockstar catalog at $z = 0$ and determine $\eta(r)$ from this sample by repeating the whole process described in the above. Note that the sample of the galactic halos includes the subhalos embedded in larger distinct halos as well as the distinct DM halos with no subhalos. The former correspond to the cluster/group galaxies while the latter to the field galaxies.

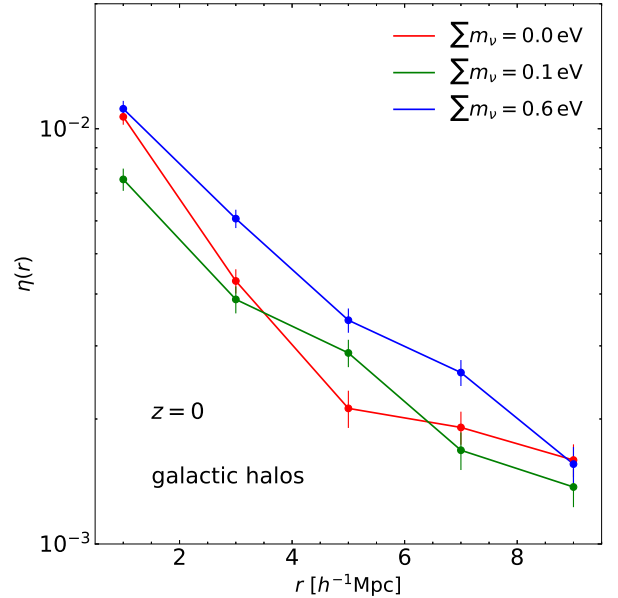


FIG. 2: Same as Figure 1 but for the galactic halos in the mass range of $1 \leq M_h/(10^{12} h^{-1} M_\odot) < 10$.

Figure 2 plots $\eta_{0.0}(r)$, $\eta_{0.1}(r)$ and $\eta_{0.6}(r)$ from the sample of the galactic halos. As can be seen, the results from the galactic halos are similar to those from the distinct ha-

los shown in Figure 1. We find $\eta_{0.1}(r) \ll \eta_{0.6}(r)$ in the whole range of r and $\eta_{0.1}(r) \ll \eta_{0.0}(r) \sim \eta_{0.6}(r)$ at $r \sim 1 h^{-1}\text{Mpc}$. A notable difference between the results shown in Figures 1 and 2 is that $\eta_{0.0}(r)$ changes its rate, $d\eta_{0.0}(r)/dr$, more abruptly around $r \sim 5 h^{-1}\text{Mpc}$, for the case of the galactic halos. It increases with the decrement of r much more mildly at $r > 5 h^{-1}\text{Mpc}$ and much more rapidly at $r \leq 5 h^{-1}\text{Mpc}$ than $\eta_{0.1}(r)$ and $\eta_{0.6}(r)$. Note that $\eta_{0.0}(r)$ is substantially lower than $\eta_{0.1}(r)$ at $r \sim 5 h^{-1}\text{Mpc}$ while it is significantly higher than $\eta_{0.1}(r)$ at $r \sim 1 h^{-1}\text{Mpc}$.

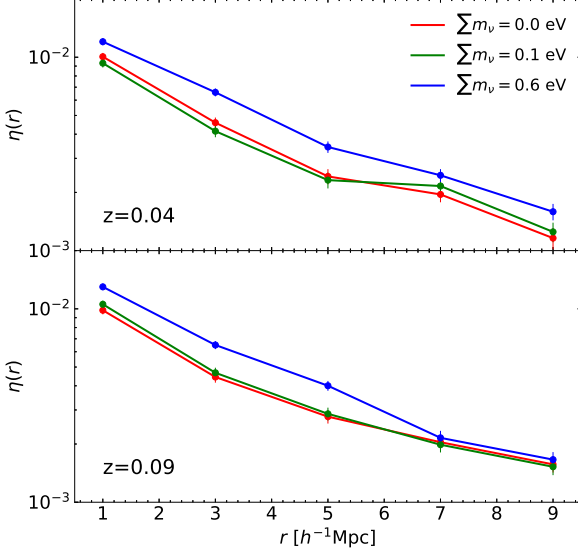


FIG. 3: Same as Figure 2 but at $z = 0.04$ (top panel) and at $z = 0.09$ (bottom panel).

We also investigate how $\eta_{0.0}(r)$, $\eta_{0.1}(r)$ and $\eta_{0.6}(r)$ from the galactic halos evolve with redshifts, by conducting the same analysis at two higher redshifts, $z = 0.04$ and 0.09 , the results of which are shown in the top and bottom panels of Figure 3, respectively. As can be seen, we find $\eta_{0.0}(r) \sim \eta_{0.1}(r) \ll \eta_{0.6}(r)$ in the whole range of r at both of the higher redshifts, which trends are well explained by the differences in σ_8 among the three models. Note also that $\eta_{0.0}(r)$ is closer to $\eta_{0.1}(r)$ in the whole range of r at $z = 0.09$ than at $z = 0.04$. This result indicates that the mechanism responsible for the significant deviation of $\eta_{0.0}(r)$ from $\eta_{0.1}(r)$ in the range of $r \leq 5 h^{-1}\text{Mpc}$ at $z = 0$ should operate much less effectively at higher redshifts.

Since the strength of the halo shape-shape correlations has been known to depend on the physical properties of the halos such as their masses, sphericities and formation epochs [13], we would like to see whether or not the differences in $\eta(r)$ among the three $\nu\Lambda\text{CDM}$ models are due to their differences in the distributions of the halo properties. Splitting the logarithmic mass range, $12 \leq \log M_h < 13$ into multiple differential bins and counting the numbers of the galactic halos whose logarithmic masses fall in each bin for each

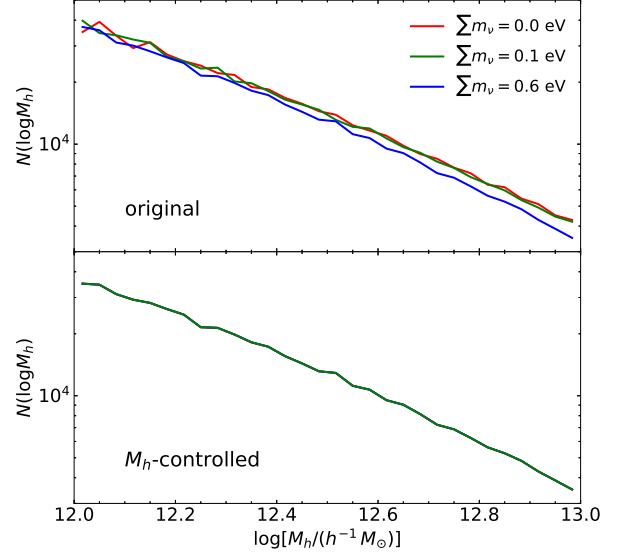


FIG. 4: Number distributions of the galactic halos at $z = 0$ from the original (top panel) and mass-controlled (bottom panel) samples for the three $\nu\Lambda\text{CDM}$ models.

of the three $\nu\Lambda\text{CDM}$ models, we determine the number distributions, $n(\log M_h)$, of the galactic halos as a function of $\log M_h$ at $z = 0$, the results of which are shown in the top panel of Figure 4. As expected, the model with heavy neutrinos exhibits the lowest amplitude of $n(\log M_h)$, while the other two models yield quite similar mass distributions.

Let $n_{0.0}(\log M_h)$, $n_{0.1}(\log M_h)$ and $n_{0.6}(\log M_h)$ denote the mass distributions of the galactic halos for the models with massless, light and heavy neutrinos, respectively. Defining n_{\min} as $n_{\min} \equiv \min\{n_{0.0}, n_{0.1}, n_{0.6}\}$, we select n_{\min} galactic halos at each mass bin from each model to create three controlled samples of the galactic halos that have identical mass distributions, which are shown in the bottom panel of Figure 4. Using these three controlled samples, we refollow the whole procedure to redetermine $\eta_{0.0}(r)$, $\eta_{0.1}(r)$ and $\eta_{0.6}(r)$ at $z = 0$ and show the results in Figure 5. As can be seen, no appreciable difference is found between the results from the original and controlled samples. Even though the three controlled samples have the identical mass distributions, they still exhibit significant differences in $\eta(r)$, which indicates that the differences in $n(\log M_h)$ are not responsible for the differences among $\eta_{0.0}(r)$, $\eta_{0.1}(r)$, $\eta_{0.6}(r)$.

In a similar manner, we also create three controlled samples of the galactic halos, which have the identical distributions of the sphericity, S , of the galactic halos, where S is defined as the minor to major axial ratio of a galactic halo [14]. Figure 6 plots the S -distributions from the original and controlled samples of the galactic halos for the three $\nu\Lambda\text{CDM}$ models at $z = 0$. As can be seen in the top panel, the galactic halos in the model with heavy neutrinos tend to be more aspherical than those in the other two models. Figure 7 plots

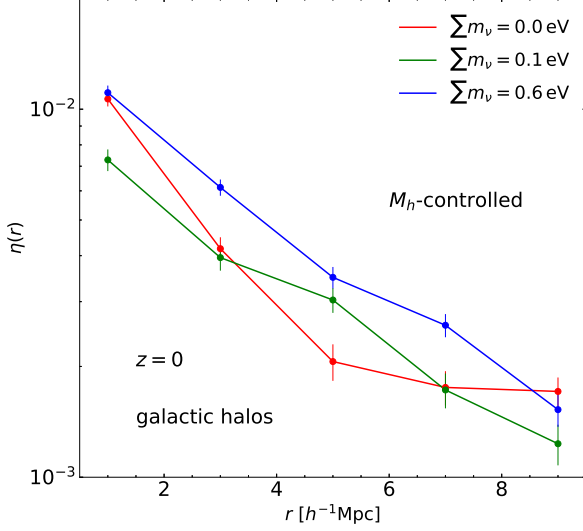


FIG. 5: Same as Figure 2 but from the M_h -controlled samples.

$\eta_{0.0}(r)$, $\eta_{0.1}(r)$, $\eta_{0.6}(r)$ from the S -controlled samples, revealing that although differences between $\eta_{0.1}(r)$ and $\eta_{0.6}(r)$ in the whole range of r is reduced compared with the results from the original sample, the controlled samples still exhibit the same degree of the key differences between $\eta_{0.0}(r)$ and $\eta_{0.1}(r)$ at $r \sim 1 h^{-1}\text{Mpc}$ as well as between $\eta_{0.0}(r)$ and $\eta_{0.6}(r)$ at $r \sim 3 h^{-1}\text{Mpc}$. This result implies that the M_ν -dependence of $\eta(r)$ cannot be ascribed to the differences in the S -distributions among the three models.

Similarly, we also examine if and how the differences in the formation epochs of the galactic halos, c_p , among the three models contribute to the differences in $\eta_{0.0}(r)$, $\eta_{0.1}(r)$, $\eta_{0.6}(r)$, where the formation epoch of a galactic halo is determined as $c_p \equiv r_s/r_v$. The c_p -distributions from the original and controlled samples for the three models are shown in Figure 8, which reveals that the galactic halos in the model with heavy neutrinos tend to have lower formation epochs than those in the other two models, as expected. The results of $\eta_{0.0}(r)$, $\eta_{0.1}(r)$, $\eta_{0.6}(r)$ from the three c_p -controlled samples are depicted in Figure 9. Note that while the difference between $\eta_{0.0}(r)$ and $\eta_{0.1}(r)$ at $r \sim 5 h^{-1}\text{Mpc}$ is substantially reduced, the difference between $\eta_{0.0}(r)$ and $\eta_{0.1}(r)$ at $r \sim 1 h^{-1}\text{Mpc}$ as well as that between $\eta_{0.0}(r)$ and $\eta_{0.6}(r)$ at $r \sim 3 h^{-1}\text{Mpc}$ is still quite significant, even when the c_p -controlled samples are used. This result implies that the differences in the c_p -distributions among the three models have little to do with the differences between $\eta_{0.0}(r)$ and $\eta_{0.1}(r)$ at $r \sim 1 h^{-1}\text{Mpc}$ nor between $\eta_{0.0}(r)$ and $\eta_{0.6}(r)$ at $r \sim 3 h^{-1}\text{Mpc}$, while they should be largely responsible for the differences between $\eta_{0.0}(r)$ and $\eta_{0.1}(r)$ at $r \sim 5 h^{-1}\text{Mpc}$.

Now that we have numerically found a robust evidence for the M_ν -dependence of $\eta(r)$ that cannot be attributed to its σ_8 -dependence, we would like to assess how detectable the

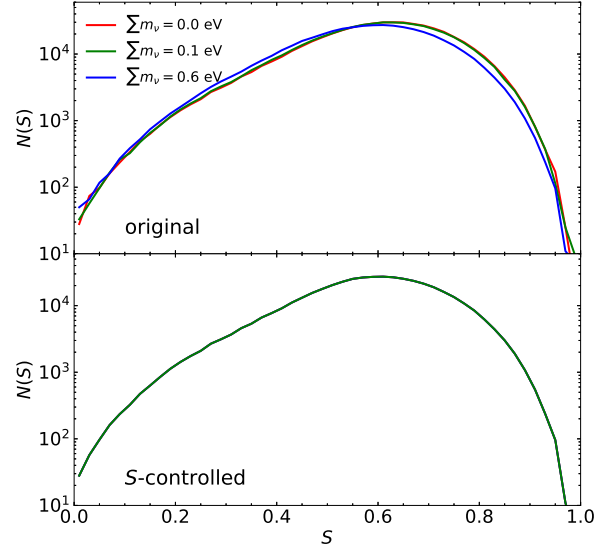


FIG. 6: Number distributions of the galactic halos at $z = 0$ from the original (top panel) and sphericity-controlled (bottom panel) samples for the three $\nu\Lambda\text{CDM}$ models.

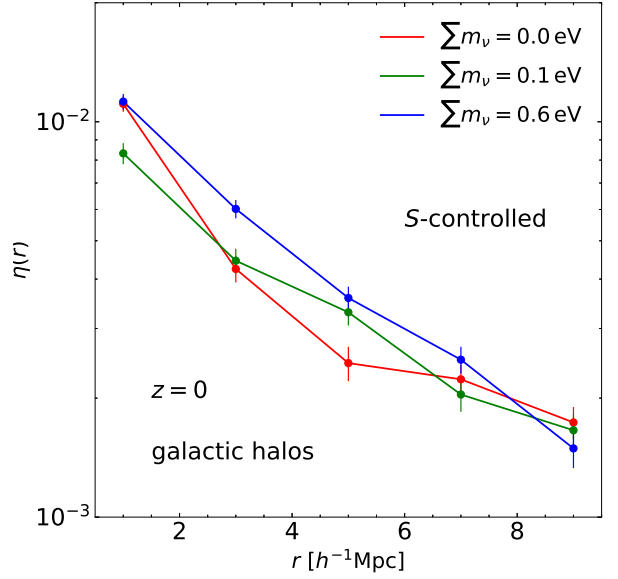


FIG. 7: Same as Figure 2 but from the S -controlled samples.

signal is in practice. Regarding the direction of the \hat{x}_3 -axis as a direction of the line of sight normal to the flat plane of the sky, we project \hat{e} onto the \hat{x}_1 - \hat{x}_2 plane and renormalize it to obtain a two dimensional unit shape vector, \hat{e}_{2d} . Then, we determine the two-dimensional shape-shape correlation function as $\eta_{2d}(r) \equiv \langle |\hat{e}_2(\mathbf{x}) \cdot \hat{e}_{2d}(\mathbf{x} + \mathbf{r})|^2 \rangle - 1/2$ for each of

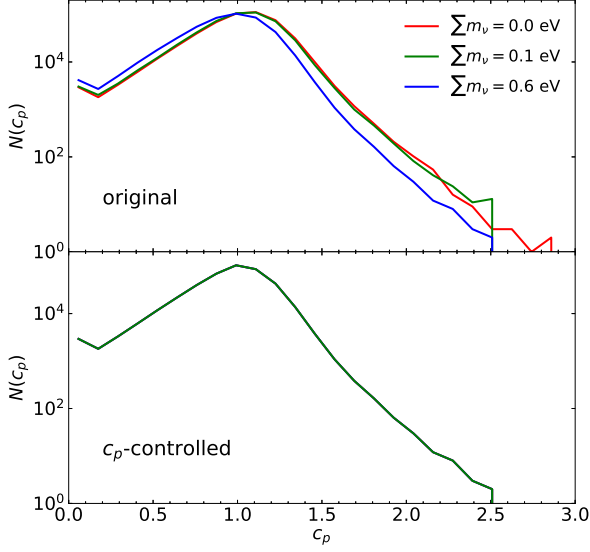


FIG. 8: Number distributions of the galactic halos at $z = 0$ from the original (top panel) and concentration parameter-controlled (bottom panel) samples for the three $\nu\Lambda$ CDM models.

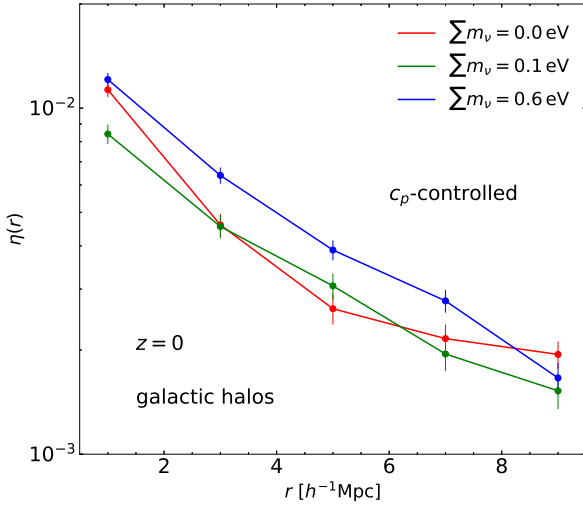


FIG. 9: Same as Figure 2 but from the c_p -controlled samples.

the three $\nu\Lambda$ CDM models. The four panels of Figure 10 plots $\eta_{2d}(r)$ from the original, M_h -controlled, S -controlled and c_p controlled samples for the three models. Although $\eta_{2d}(r)$ carries large errors compared with $\eta(r)$ in the whole range of r , the differences between $\eta_{2d,0.0}$ and $\eta_{2d,0.1}$ at $r \sim 1 h^{-1}\text{Mpc}$ seem to remain significant for all of the four cases.

To assess more rigorously the statistical significance, we perform the KolmogorovSmirnov (KS) test of the null hypothesis that there is no difference between $\eta_{2d,0.0}$ and $\eta_{2d,0.1}$ at

$r \sim 1 h^{-1}\text{Mpc}$. For this KS test, we first determine the cumulative probability distribution, $P(< \cos \theta_{2d})$, with $\cos \theta_{2d} \equiv |\hat{\mathbf{e}}_{2d}(\mathbf{x}) \cdot \hat{\mathbf{e}}_{2d}(\mathbf{x} + \mathbf{r})|$ with $|\mathbf{r}| = 1 h^{-1}\text{Mpc}$ for each sample. If $\hat{\mathbf{e}}_{2d}$ is completely random, then $P(< \cos \theta_{2d}) = \cos \theta_{2d}$. If $\hat{\mathbf{e}}_{2d}$ is cross-correlated, then $P(< \cos \theta_{2d}) < \cos \theta_{2d}$ in the range of $0 < \cos \theta_{2d} < 1$. The stronger the cross-correlations are, the smaller $P(< \cos \theta_{2d})$ is than $\cos \theta_{2d}$. We calculate the KS statistics as $\max |P_{0.0} - P_{0.1}|$, where $P_{0.0}$ and $P_{0.1}$ represent $P(< \cos \theta_{2d})$ from the models with massless and light neutrinos, respectively, and evaluate the confidence level at which the null hypothesis is rejected with this KS statistics.

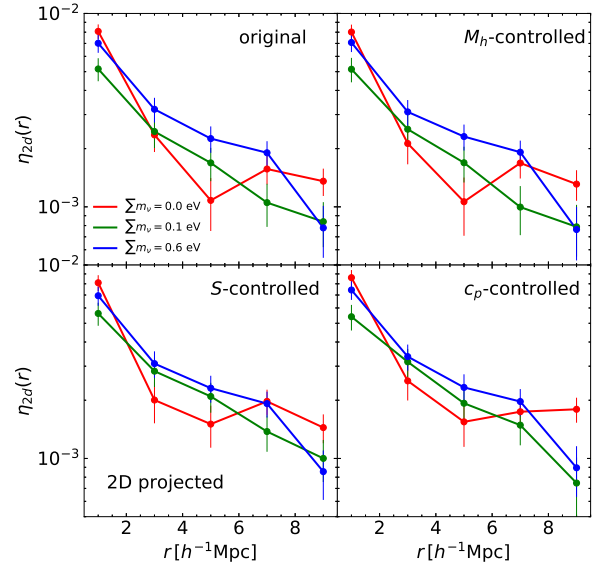


FIG. 10: Same as Figure 2 but for the case that the shape vectors are projected onto the 2D plane.

Figure 11 plots $\cos \theta_{2d} - P(< \cos \theta_{2d})$ obtained from the pairs of the galactic halos with separation distance $r \sim 1 h^{-1}\text{Mpc}$ belonging to the original, M_h -controlled, S -controlled and c_p controlled samples for the two $\nu\Lambda$ CDM models with massless and light neutrinos. As can be seen, the KS statistics are large enough to reject the null hypothesis at the confidence level higher than 99.9% for all of the four cases. In other words, the two models with massless and light neutrinos significantly differ in the strengths of the cross-correlations of the projected shapes of the galactic halos at $r \sim 1 h^{-1}\text{Mpc}$. It is worth mentioning that the statistical significance of the differences between $\eta_{0.0}(r)$ and $\eta_{0.6}(r)$ at $3 h^{-1}\text{Mpc}$, however, seems to be severely reduced by the projection effects. A larger sample of the galaxies should be required to beat down the projection effects for the detection of this signal in practice.

Discussions and Conclusion. We have numerically determined the galaxy shape-shape correlation functions, $\eta(r)$, by analyzing the data from the MassiveNuS for three different $\nu\Lambda$ CDM models with $M_\nu = 0.0, 0.1, 0.6 \text{ eV}$. It has been shown that the three models significantly differ in $\eta(r)$

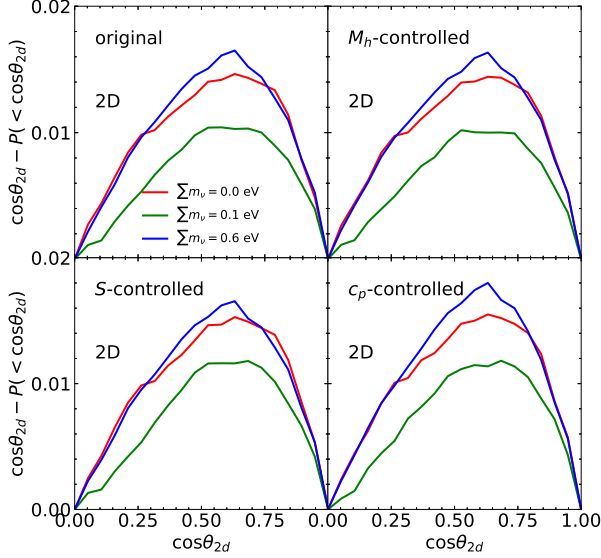


FIG. 11: Differences between $\cos\theta_{2d}$ and $P(< \cos\theta_{2d})$ from the original, M_h -controlled, S -controlled and c_p -controlled samples of the galactic halos for the three $\nu\Lambda\text{CDM}$ models.

at $r \leq 5 h^{-1}\text{Mpc}$ among one another, which implies that $\eta(r)$ should be in principle a powerful new probe of M_ν .

The robustness of this new probe has been tested against controlling the properties of the galactic halos that are correlated with the strengths of $\eta(r)$. Even when the correlations are measured from the projected shapes of the galactic halos

in the two dimensional space, the differences among the three models at $r \leq 5 h^{-1}\text{Mpc}$ have been found to statistically significant.

The galaxy shape-shape correlation has two advantages as a complementary probe of M_ν . First, it is sensitive enough to distinguish between $M_\nu = 0.0$ and 0.1 eV . Second, it has a potential to break the σ_8 - M_ν degeneracy since the differences in $\eta(r)$ among the three models cannot be explained by the differences in σ_8 .

A backup work, however, has to be done before making a practical use of $\eta(r)$ as a probe of M_ν . For a direct comparison with observational data, it will be necessary to determine the shape vectors of the galaxies and their cross-correlations from their baryonic gas particles, for which the data from the cosmological hydrodynamic simulations for the $\nu\Lambda\text{CDM}$ models will be required. It will be also necessary to take into proper account the effects of the misalignments between the DM and baryonic particle distributions as well as the feedbacks of the non-gravitational processes, since they could be strong enough to alter the behaviors of $\eta(r)$ [15]. Our future work will be in this direction.

Acknowledgements. We thank the Columbia Lensing group for making their suite of simulated maps available at the website (<http://columbialensing.org>), and NSF for supporting the creation of those maps through grant AST-1210877 and XSEDE allocation AST-140041. We thank the New Mexico State University (USA) and Instituto de Astrofísica de Andalucía CSIC (Spain) for hosting the Skies & Universes site for cosmological simulation products. We acknowledge the support by Basic Science Research Program through the National Research Foundation (NRF) of Korea funded by the Ministry of Education (No.2019R1A2C1083855).

-
- [1] M. Brown, A. Taylor, N. Hambly and S. Dye, Mon. Not. Roy. Astron. Soc. **333**, 501 (2002) ; T. Okumura, Y. Jing and C. Li, Astrophys. J. **694**, 214-221 (2009)
 - [2] C. A. Vera-Ciro, *et al.* Mon. Not. Roy. Astron. Soc. **416**, 1377-1391 (2011)
 - [3] H. Y. Wang, *et al.* Mon. Not. Roy. Astron. Soc. **364**, 424-432 (2005) ; X. Kang and P. Wang, Astrophys. J. **813**, no.1, 6 (2015)
 - [4] M. Borzyszkowski, *et al.* Mon. Not. Roy. Astron. Soc. **469**, no.1, 594-611 (2017)
 - [5] J. R. Bond, L. Kofman and D. Pogosyan, Nature **380**, 603-606 (1996)
 - [6] J. Lesgourgues and S. Pastor, Adv. High Energy Phys. **2012**, 608515 (2012) ; J. Lesgourgues and S. Pastor, New J. Phys. **16**, 065002 (2014)
 - [7] S. Ryu and J. Lee, Astrophys. J. **894**, 65 (2020) ; J. Lee, N. I. Libeskind and S. Ryu, [arXiv:2004.02638 [astro-ph.CO]].
 - [8] M. C. Gonzalez-Garcia and M. Maltoni, Phys. Rept. **460**, 1 (2008)
 - [9] J. Lee, V. Springel, U. L. Pen and G. Lemson, Mon. Not. Roy. Astron. Soc. **389**, 1266-1274 (2008)
 - [10] J. Liu, *et al.* JCAP **1803**, 049 (2018)
 - [11] P. S. Behroozi, R. H. Wechsler and H. Y. Wu, Astrophys. J. **762**, 109 (2013)
 - [12] U. L. Pen, J. Lee and U. Seljak, Astrophys. J. Lett. **543**, L107 (2000) ; J. Lee and U. L. Pen, Astrophys. J. **555**, 106-124 (2001)
 - [13] Q. Xia, *et al.* Astrophys. J. **848**, no.1, 22 (2017) ; D. Piras, *et al.* Mon. Not. Roy. Astron. Soc. **474**, no.1, 1165-1175 (2018) ;
 - [14] P. Bett, V. Eke, C. S. Frenk, A. Jenkins, J. Helly and J. Navarro, Mon. Not. Roy. Astron. Soc. **376**, 215-232 (2007)
 - [15] M. Velliscig, *et al.* Mon. Not. Roy. Astron. Soc. **454**, no.3, 3328-3340 (2015) ; A. Tenneti, R. Mandelbaum, T. Di Matteo, A. Kiessling and N. Khandai, Mon. Not. Roy. Astron. Soc. **453**, no.1, 469-482 (2015) ; S. Hilbert, D. Xu, P. Schneider, V. Springel, M. Vogelsberger and L. Hernquist, Mon. Not. Roy. Astron. Soc. **468**, no.1, 790-823 (2017) ; A. Tenneti, N. Y. Gnedin and Y. Feng, Astrophys. J. **834**, no.2, 169 (2017)